Magnetic excitations in the metallic single-layer ruthenates $Ca_{2-x}Sr_xRuO_4$ studied by inelastic neutron scattering

P. Steffens,[1,2,*] O. Friedt,[1] Y. Sidis,[3] P. Link,[4,†] J. Kulda,[2] K. Schmalzl,[5] S. Nakatsuji,[6] and M. Braden[1,‡]

[1]*II. Physikalisches Institut, Universität zu Köln, Zülpicher Strasse 77, D-50937 Köln, Germany*

[2]*Institut Laue Langevin, 6 Rue Jules Horowitz BP 156, F-38042 Grenoble Cedex 9, France*

[3]*Laboratoire Léon Brillouin, Centre d'Etudes Atomiques/Centre National de la Recherche Scientifique (CEA/CNRS), F-91191 Gif-sur-Yvette Cedex, France*

[4]*Forschungsneutronenquelle Heinz Maier-Leibnitz (FRM-II), TU München, Lichtenbergstrasse 1, D-85747 Garching, Germany*

[5]*Institute of Solid State Research (IFF), Forschungszentrum Jülich GmbH, Jülich Centre for Neutron Science (JCNS) at Institut Laue-Langevin (ILL), F-38042 Grenoble Cedex 9, France*

[6]*Institute for Solid State Physics, University of Tokyo, Kashiwa, Chiba 277-8581, Japan*

(Received 22 April 2010; revised manuscript received 8 December 2010; published 24 February 2011)

By inelastic neutron scattering, we have analyzed the magnetic correlations in the paramagnetic metallic region of the series $Ca_{2-x}Sr_xRuO_4$, $0.2 \leqslant x \leqslant 0.62$. We find different contributions that correspond to two-dimensional ferromagnetic fluctuations and to fluctuations at incommensurate wave vectors $Q_1^{IC} = (0.11,0,0)$, $Q_2^{IC} = (0.26,0,0)$, and $Q_{\alpha\beta}^{IC} = (0.3,0.3,0)$. These components constitute the measured response as a function of the Sr concentration x, of the magnetic field, and of the temperature. A generic model is applicable to metallic $Ca_{2-x}Sr_xRuO_4$ close to the Mott transition, in spite of their strongly varying physical properties. The amplitude, characteristic energy, and width of the incommensurate components vary only slightly as functions of x, but the ferromagnetic component depends sensitively on concentration, temperature, and magnetic field. While ferromagnetic fluctuations are very strong in $Ca_{1.38}Sr_{0.62}RuO_4$ with a low characteristic energy of 0.2 meV at $T = 1.5$ K, they are strongly suppressed in $Ca_{1.8}Sr_{0.2}RuO_4$, but reappear upon the application of a magnetic field, and form a magnon mode above the metamagnetic transition. The inelastic neutron scattering results document how the competition between ferromagnetic and incommensurate antiferromagnetic instabilities governs the physics of this system.

DOI: 10.1103/PhysRevB.83.054429 PACS number(s): 74.70.Pq, 75.30.Kz, 74.20.Mn, 78.70.Nx

I. INTRODUCTION

The family of layered ruthenates has been the focus of interest since the discovery of superconductivity in Sr_2RuO_4 (Refs. 1 and 2) whose unconventional nature is still being investigated. The series $Ca_{2-x}Sr_xRuO_4$, which arises from Sr_2RuO_4 by substitution of Sr by Ca, exhibits a variety of exciting phenomena on its own. Although the replacement of Sr by Ca does not change the number of charge carriers, the electronic and magnetic behavior is closely coupled to slight structural changes and varies considerably as a function of the Sr content x.[3,4] Ca_2RuO_4 is a Mott insulator and is antiferromagnetically ordered below 110 K,[5,6] while for $x > 0.18$, the ground state is metallic. The strongly enhanced values of the magnetic susceptibility indicate that the system is close to a ferromagnetic instability at approximately $x = 0.5$.[3] $Ca_{2-x}Sr_xRuO_4$ samples with $x \sim 0.5$ exhibit a remarkably large value of the Sommerfeld coefficient of the specific heat in the range of heavy-fermion compounds. Moreover, for $0.2 < x < 0.5$, a metamagnetic transition from a state with low susceptibility, reminiscent of antiferromagnetic correlations, to a state with high magnetic polarization is observed.[7,8] The metamagnetic transition is also observed in the closely related bilayer ruthenate $Sr_3Ru_2O_7$,[9] where a discussion about its quantum-critical behavior has generated further interest. The high concentration dependence of the ground state in $Ca_{2-x}Sr_xRuO_4$ points to a complex interplay of distinct magnetic correlations. A precise characterization of the magnetic excitations in the layered ruthenates seems interesting owing to several reasons: First, ferromagnetic fluctuations are considered to play an important role in the superconducting pairing in Sr_2RuO_4. As ferromagnetic fluctuations are difficult to study in this material, insight can be more easily gained from the $Ca_{2-x}Sr_xRuO_4$ compounds. In addition, the complex magnetism in $Ca_{2-x}Sr_xRuO_4$ arises from the interplay between structural and orbital degrees of freedom, which is relevant in many transition-metal oxides. An orbital-selective Mott transition has been proposed to explain the fascinating magnetism in $Ca_{2-x}Sr_xRuO_4$.[10]

Before we discuss the experimental findings, we briefly introduce the general concepts to describe magnetic fluctuations in itinerant magnets, and we summarize previous studies on magnetic correlations in layered ruthenates, introducing the magnetic contributions to the magnetic scattering in $Ca_{2-x}Sr_xRuO_4$ by the aid of an intensity map measured for $x = 0.2$. We then discuss in separate sections the three antiferromagnetic and the ferromagnetic components of the excitation spectrum in $Ca_{2-x}Sr_xRuO_4$ with $0.2 \leqslant x \leqslant 0.62$, and finally we analyze the effect of magnetic fields on these correlations.

II. NEUTRON SCATTERING ON MAGNETIC FLUCTUATIONS IN ITINERANT MAGNETS

Magnetic inelastic neutron scattering (INS) measures the imaginary part of the susceptibility as function of wave vector and of frequency (energy transfer $\hbar\omega$). The cross section is given by[11]

$$\frac{d^2\sigma}{d\Omega\, d\omega} \propto \frac{F^2(\mathbf{Q})}{1 - \exp\left(-\frac{\hbar\omega}{k_B T}\right)} \chi''(\mathbf{Q},\omega), \qquad (1)$$

where $F(\mathbf{Q})$ is the magnetic form factor.

The spin dynamics in itinerant paramagnetic systems such as the layered ruthenates has the character of fluctuations, i.e., correlations limited in space and in time, around the paramagnetic ground state. χ'' is nonzero in large portions of $\mathbf{Q},\omega$ space, and it is the structure inside this excitation continuum that contains information about the magnetic interactions.

In principle, one may analytically calculate the susceptibility χ'' via the Lindhard function, i.e., by a sum over all possible excitations of electrons from occupied into empty states, and by taking into account correlation effects via an additional interaction parameter (see, for instance, Ref. 12). If this is not feasible owing to insufficient knowledge about the electronic band structure, one may still use more general expressions for χ'' that are valid near the ferromagnetic or antiferromagnetic instabilities. Expanding the inverse susceptibility as $\chi_q^{-1}(1 - i\omega/\Gamma_q)$ (see Refs. 12 and 13), the imaginary part of the susceptibility is conveniently written in the form

$$\chi''(q,\omega) = \chi_q \frac{\omega\Gamma_q}{\omega^2 + \Gamma_q^2}. \tag{2}$$

At different q, the frequency spectrum has thus qualitatively the same form, which frequently is referred to as a "(single) relaxor" in the literature, and which has its maximum at $\omega = \Gamma_q$.

χ_q is expressed as $\chi_q = \frac{\chi}{1+\xi^2(q-q_o)^2}$. The form of Γ_q depends on the nature of the magnetic instability, i.e., if it is ferromagnetic (propagation vector $q_0 = 0$) or antiferromagnetic (all $q_0 \neq 0$, i.e., possibly incommensurate). In the ferromagnetic case, one obtains

$$\Gamma_q = \Gamma_0 \xi q(1 + \xi^2 q^2), \tag{3}$$

while in the antiferromagnetic case

$$\Gamma_q = \Gamma_0(1 + \xi^2(q - q_0)^2). \tag{4}$$

The parameters Γ_0 and ξ depend on the microscopic details and on how close the system is to the magnetic phase transition. From the phenomenological point of view, they can be used to parametrize the magnetic fluctuations in $\mathbf{Q},\omega$ space in a convenient and remarkably simple way. ξ defines the length scale, which may be regarded as a correlation length, and Γ_0 defines the energy scale.

The additional factor q in (3) causes Γ_q to vanish for $q \to 0$, which implies that the shape of $\chi''(q,\omega)$, despite its continuum character, resembles that of a dispersive excitation. (Owing to its vague resemblance to a magnon in the ordered state, such an excitation is often called a paramagnon.) In contrast, there is no dispersive feature in the antiferromagnetic case (4); it is maximum at (q_0,Γ_0).

An illustration of how the intensity is distributed in both cases will be given in the context of the discussion of the experimental results later on (see Sec. VI).

III. SAMPLES AND EXPERIMENTAL ASPECTS

Owing to the limitations by neutron flux and by signal strength, large samples are necessary to study magnetic excitations in layered ruthenates by INS. The experiments have been performed on single crystals of $Ca_{2-x}Sr_xRuO_4$ with concentrations $x = 0.2$ and 0.62, which have been obtained by a floating zone method at the University of Kyoto and had masses of 1.9 and 1.8 g, respectively.

Different triple-axis spectrometers have been used: 4F1, 4F2, 1T, and 2T at the LLB, Saclay, IN14, IN12, IN22, and IN20 at the ILL, Grenoble, and Panda at FRM-II, Garching. On the thermal neutron spectrometers 1T, 2T, and IN22 we used a fixed final neutron wave vector $k_f = 2.662$ Å^{-1} and graphite filters. On IN20 we have used the newly available Flatcone multidetector with $k_f = 3$ Å^{-1} in order to obtain a mapping of the intensity distribution.[14] On the cold neutron spectrometers (unless otherwise stated) k_f has been set to 1.5 Å^{-1} and beryllium filters were used to suppress higher orders. In all cases, focusing monochromators and analyzers have been employed. Magnetic fields up to 10 T have been applied using vertical cryomagnets.

In order to access different regions in reciprocal space, the samples have been mounted either in a [100]-[010] orientation, i.e., with $a^\star$ and $b^\star$ in the scattering plane, or in a [100]-[001] orientation that gives access to momentum transfers along $c^\star$. Here and in the following, the notation is based on a unit cell that corresponds to that of Sr_2RuO_4, i.e., $a = b =$ 3.76 Å, and $c = 12.65$ Å for $x = 0.62$ and $c = 12.55$ Å for $x = 0.2$. This notation neglects the structural distortions—a rotation of the RuO_6 octahedra around the vertical axis and an additional tilt in the case of $x = 0.2$ (Ref. 15)—that have to be described in a larger unit cell ($\sqrt{2}a\ \sqrt{2}a\ 2c$). Samples were well characterized by neutron diffraction; in particular, by regarding characteristic superstructure reflections of the structural distortions, we can state that the $Ca_{1.8}Sr_{0.2}RuO_4$ sample was twinned with approximately equal amounts of both twins. This compound is orthorhombic with a small splitting of the in-plane lattice constants owing to the tilt distortion. Furthermore, we verified that the structure corresponds to the so-called D-Pbca phase and not to the L-Pbca phase, which is in close proximity in the phase diagram.[15] (These two structural phases correspond to the two possible senses of rotation of next-nearest layers with respect to each other; it is the same in L-Pbca and opposite in D-Pbca, which causes a doubling of the c lattice parameter.[15])

All measurements were carried out with unpolarized neutron beams. Phonon scattering should not occur in our experiments, as no optical phonons exist in the analyzed energy and q range,[16] and the contamination by acoustic phonons is avoided when working around $Q = (1,0,0)$. There is no Bragg scattering at this Q point because of the symmetry of the crystal structure (including the distortions), but as argued below, (1,0,0) can nevertheless be considered as a magnetic zone center. The measured signals are consistent to the previous results on magnetic excitations in the ruthenates (for instance, Refs. 17–19), and studies of the Q and temperature dependence further corroborate the magnetic character. Using the lattice dynamical model described in Ref. 16, we may calculate the distribution of the dynamic structure factor of an acoustic phonon branch at $Q = (2,0,0)$ and fold it with the experimental resolution in order to describe a phonon scan. Using the same folding for the magnetic data, it has been possible to assign absolute susceptibility units to our data.

IV. OVERVIEW ON MAGNETIC EXCITATIONS IN THE RUTHENATES

Magnetic excitations have so far been studied by INS in several layered ruthenates. The most detailed description is at present available for Sr_2RuO_4.[17,18,20–23] Furthermore, the bilayer compound $Sr_3Ru_2O_7$ has been investigated.[24–26] The excitations in these materials have the character of fluctuations that are both relatively broad in $\mathbf{Q}$ and ω. In Sr_2RuO_4, these fluctuations reside at $\mathbf{Q} = (0.3,0.3,0)$, i.e., at incommensurate wave vectors on the diagonal of the Brillouin zone. In $Sr_3Ru_2O_7$, excitations at two inequivalent wave vectors have been identified that are on the $a^\star$ (respectively $b^\star$) axis of the Brillouin zone.

Apart from a strong interaction within one double block in the case of the bilayer ruthenates, no dependence on the L component of $\mathbf{Q} = (H,K,L)$ has been found after correction for the decrease governed by the ruthenium magnetic form factor. Thus, there is no relevant magnetic correlation between moments in different RuO_2 layers, and it is sufficient to regard the two in-plane dimensions and to neglect the L component of Q. The two-dimensional (2D) Brillouin zone is quadratic, and all Q's with integers H and K are zone centers, i.e., any excitation at such Q, in particular at $(1,0,0)$ or $(0,0,L)$, is of ferromagnetic character.

In Sr_2RuO_4, the magnetic excitation at $Q^{\rm IC}_{\alpha\beta} = (0.3,0.3,L)$ is very well understood on the basis of the underlying electronic band structure;[27] the Fermi surface consists of three sheets, and $Q^{\rm IC}_{\alpha\beta}$ is the nesting vector connecting the so-called α and β sheets that arise from the ruthenium $4d_{xz}$ and $4d_{yz}$ orbitals.[27,28] In $Sr_3Ru_2O_7$, the Fermi surface is far more complex,[29,30] so it is less simple to identify which parts of it give the relevant contribution.

In the single-layer ruthenates, however, there are other wave vectors at which magnetic correlations have been observed: In $Ca_{2-x}Sr_xRuO_4$ with $x = 0.62$,[19] large contributions at the incommensurate wave vectors $(0.22,0,0)$ and equivalent ones have been observed; in $Ca_{1.8}Sr_{0.2}RuO_4$,[31] similar excitations have been seen, and even a separation in two contributions at $Q^{\rm IC}_1 = (0.12,0,0)$ and $Q^{\rm IC}_2 = (0.27,0,0)$ could be resolved. In all these respects, the Ca-doped materials $Ca_{2-x}Sr_xRuO_4$ are thus fundamentally different from Sr_2RuO_4.

Finally, ferromagnetic correlations have been identified in $Ca_{1.8}Sr_{0.2}RuO_4$ at elevated temperatures or upon application of a magnetic field.[31] To what extent ferromagnetic correlations play a role also in Sr_2RuO_4 and its superconductivity remains so far an open question.

An overview of the distribution of scattered intensity is obtained from the data in Fig. 1 taken for $Ca_{1.8}Sr_{0.2}RuO_4$, which covers a wide region of a plane in reciprocal space. The data have been obtained using the Flatcone multidetector option of the IN20 spectrometer[14] with the sample oriented in the a,b plane. By tilting the sample and by placing the detector array in an inclined position out of the horizontal plane just above the direct beam, a map of scattering vectors with a constant finite vertical component of $L = 1.4$ is obtained. The accessible horizontal components of Q (H and K) are small in this configuration, which is convenient for the study of magnetic scattering.

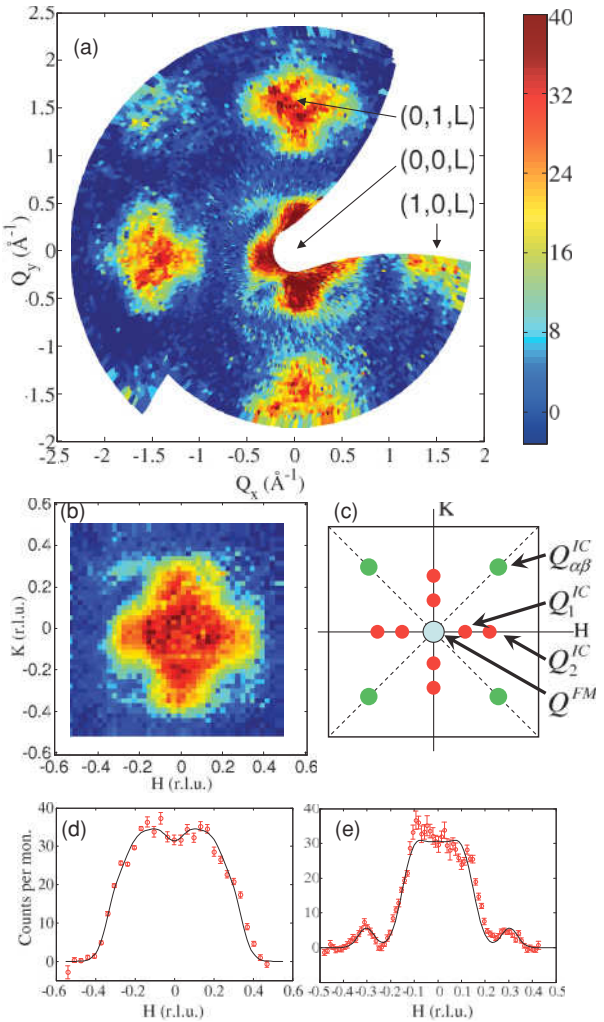

FIG. 1. (Color online) Magnetic scattering in $Ca_{1.8}Sr_{0.2}RuO_4$ at $T = 2$ K and $\Delta E = 4$ meV. (a) Intensity map over several Brillouin zones at a constant value of $L = 1.4$. A smooth background has been subtracted. Data was taken on IN20 using the flat-cone setup. (b) Magnetic scattering in one Brillouin zone, obtained from the data in (a) by projecting to the range $H,K = [-0.5,0.5]$, thereby averaging the scattering from different Brillouin zones (after correction for the Ru magnetic form factor). (c) Sketch of the (2D) Brillouin zone and the positions of the different signals. (d) Intensity along a line $Q = (H,0,1.4)$, obtained by integration of the 2D data set in (b). (e) The same for a diagonal cut through the Brillouin zone through $(0,0,1.4)$. The data in all parts of the figure are normalized to a monitor count rate that corresponds to ∼1 min counting time per point.

In the intensity map in Fig. 1(a), one clearly sees the magnetic intensity centered at the points with integer H and K, in accordance with the above discussed 2D character of the magnetic fluctuations. Owing to the magnetic form factor, the intensity is weaker as the modulus of Q is higher, i.e., in the outer regions of the map.

The sketch in Fig. 1(c) summarizes all the different positions of the signals that have been discussed in the beginning of this section (see also Ref. 31). The crosslike intensity pattern that dominates in the intensity map, in particular, when reducing it to one (2D) Brillouin zone [see Fig. 1(b)], originates

from the superposition of intensity stemming from the signals at Q_1^{IC} and Q_2^{IC}. The resolution, effectively broadened also by the averaging over several zones, is not sufficient to separate these contributions in the map, as it is well possible in the data previously collected at lower-energy transfer and with a different experimental geometry.[31] The intensity at $Q_{\alpha\beta}^{IC}$ is relatively weak compared to the one near the zone center, and therefore this $Q_{\alpha\beta}^{IC}$ signal is only weakly visible in the color plot. When integrating the 2D data set over a stripe of $\sim$0.1 Å^{-1} width that runs along the diagonal of the Brillouin zone, these signals are clearly distinguishable [Fig. 1(e)].

V. INCOMMENSURATE FLUCTUATIONS

In this section we discuss the different contributions to the incommensurate scattering that exhibit an antiferromagnetic character. The observation of peaks at $Q = (0.7,0.3,0)$ and $(1.3,0.3,0)$ in $Ca_{1.38}Sr_{0.62}RuO_4$ [see Figs. 2(a) and 2(b)] proves that the signal that arises from nesting of the α and β bands in Sr_2RuO_4 and that has been observed in $Ca_{1.8}Sr_{0.2}RuO_4$ as well (see Fig. 1 and Ref. 31) is also present for $x = 0.62$. Fitting the position of these peaks on different equivalent Q vectors yields $H,K = 0.301 \pm 0.005$, i.e., the same values as in the case of pure Sr_2RuO_4.[17] This signal thus indicates that the nesting of the α and β band remains intact despite all changes in the crystal structure and in the Fermi surfaces. First-principles calculations[32] come to the conclusion that, apart from the back-folding effect, the α and β sheets of the Fermi surface are only slightly affected by the rotational distortion of the structure.[33,34] The invariance of this nesting signal also suggests that the filling of these bands with respect to the γ band does not significantly change from the values in Sr_2RuO_4. In a simple model that assumes a rigid filling of the band structure, we calculate that an increase of the occupation number $n(\alpha) + n(\beta)$ by $\sim$0.1 electron would already shift the nesting peak more than 0.02 in H and K along the diagonal of the Brillouin zone—by far more than the maximum shift consistent with the experimental error bars. Even though the details of the real band structure might slightly change this estimation, it imposes a very low boundary of the shift of electrons among the orbitals, and is thus in clear contradiction to the proposed scenario of an orbital selective Mott transition,[10] which requires integer filling of the bands.

Figures 2(c) and 2(d) show scans along the $b^\star$ axis across $\mathbf{Q} = (1,0,0)$ for $x = 0.62$. The shape of the signal resembles closely that in $Ca_{1.8}Sr_{0.2}RuO_4$.[31] It exhibits steep edges at approximately $H = \pm 0.35$ and has, apart from a minimum in the center, a broad and flat plateau in between. These features are observed in scans at a number of different energy transfers and temperatures. A satisfactory fit thus *cannot* be performed with a single symmetric (Gaussian) contribution of whatever width, but requires at least two contributions on both sides. A fit using symmetric Gaussian peaks yields the positions $q_1 = (1,0.10 \pm 0.01,0)$ and $q_2 = (1,0.26 \pm 0.01,0)$, which are nearly the same values as those reported for $Ca_{1.8}Sr_{0.2}RuO_4$.[31]

The obtained description of the data is fully satisfying for $Ca_{1.38}Sr_{0.62}RuO_4$ as well as for $Ca_{1.8}Sr_{0.2}RuO_4$; furthermore, the description is consistent for both cases. The large width and the significant overlap of the single contributions do not allow us to resolve if there are even more structures intrinsic to these fluctuations or not. At least an additional ferromagnetic component, which is discussed in detail in the next section, still plays some role at this energy and is the likely origin of the less well-pronounced minimum at (1,0,0) and the slightly lower q_1 in comparison to $Ca_{1.8}Sr_{0.2}RuO_4$.

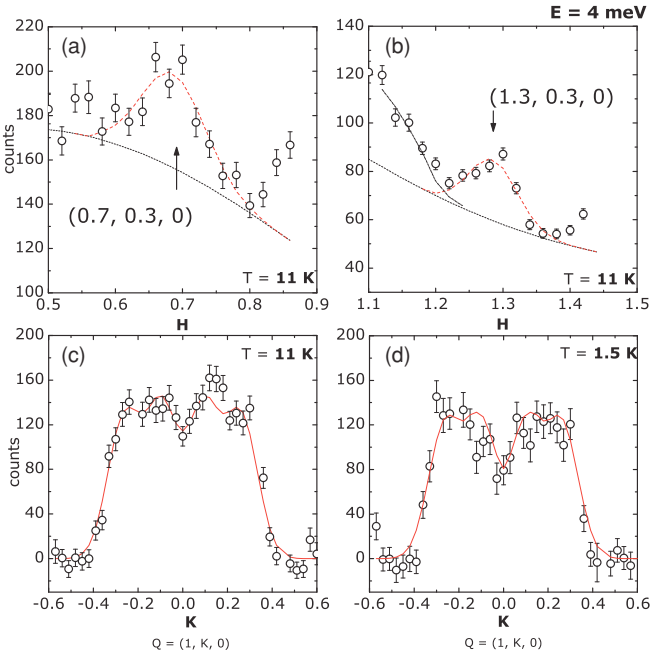

FIG. 2. (Color online) Incommensurate signals in $Ca_{1.38}Sr_{0.62}RuO_4$. (a) and (b) Diagonal scans across $Q_{\alpha\beta}^{IC}$; the thin dotted line is the scattering-angle-dependent background. (c) and (d) Transverse scans (background subtracted) across (1,0,0), crossing the positions Q_1^{IC} and Q_2^{IC} at two temperatures. Scans were taken with an energy transfer of 4 meV on the 1T spectrometer.

A. Relation between incommensurate signals and the Fermi surface

It appears most interesting to associate the different incommensurate scattering contributions with nested parts of the Fermi surface, similar to the case of the excitations at $Q_{\alpha\beta}^{IC}$ in Sr_2RuO_4. The analysis for $Ca_{2-x}Sr_xRuO_4$ is, however, much more difficult because the structural distortions and the large unit cell render the Fermi surface very complex, and the present knowledge about the Fermi surface in $Ca_{2-x}Sr_xRuO_4$ is insufficient to clearly assign the origin of the Q_1^{IC} and Q_2^{IC} peaks.

There seems to be an overall consensus concerning the electronic structure of the two end members, Sr_2RuO_4 and Ca_2RuO_4. In Sr_2RuO_4 the four electrons are equally distributed amongst the three t_{2g} bands, yielding a filling of 2/3 for the three orbitals.[33,34] For this electronic arrangement the van Hove singularity near $q = (0,0.5,0)$ in the γ band associated with the d_{xy} orbitals is situated only slightly above the Fermi energy. On the other side of the phase diagram, the Mott state in Ca_2RuO_4 is associated with orbital ordering driven through the strong structural changes. The pronounced flattening of the octahedron in Ca_2RuO_4 (Ref. 35) results in a full occupation

of the d_{xy} orbitals and in half-filled d_{xz}- and d_{yz}-orbital states undergoing the Mott transition.[33,34,36,37] Qualitatively this picture of orbital order seems to be valid for all $Ca_{2-x}Sr_xRuO_4$ undergoing the metal-insulator transition, i.e., for $x < 0.2$. The electronic structure of the metallic samples with a slightly larger Sr content studied here remains a matter of controversy both in experiment and in theory. Anisimov *et al.*[10] proposed an orbital-selective Mott transition with the idea that correlations should first result in a localization of the d_{xz} and d_{yz} states, because the corresponding bands exhibit a smaller bandwidth in pure Sr_2RuO_4. The rotation of the octahedra around the c axis, however, is found to strongly influence the γ band associated with the d_{xy} orbitals owing to the variation of the hopping.[33,34] The d_{xy} band essentially flattens with the rotation and slightly shifts to lower energies whereas the d_{xz} and d_{yz} bands are only slightly affected.[32–34,37] The Fermi surface associated with the d_{xy} band undergoes a topological transition, as the van Hove singularity shifts from above to below the Fermi level, so that the character of this band becomes holelike. The electronic band-structure calculations hence suggest that the γ band associated with the d_{xy} orbitals is much closer to localization than the other bands, in disagreement with the initial idea of an orbital selective Mott transition in the d_{xz}-d_{yz} orbitals.[10]

There is strong experimental evidence that the anomalous properties of $Ca_{2-x}Sr_xRuO_4$ with $x \sim 0.5$ are mainly associated with the γ band and with the d_{xy} orbitals. A spin-density study on $Ca_{1.5}Sr_{0.5}RuO_4$ directly proves that the high magnetic polarization in these phases arises from the d_{xy} orbitals,[38] which are hybridized with in-plane oxygen orbitals. Optical spectroscopy also identifies the d_{xy}-band renormalization as the origin of the heavy-mass behavior in $Ca_{1.5}Sr_{0.5}RuO_4$.[39] Furthermore, several angle-resolved photoemission spectroscopy (ARPES) measurements confirm the essential modification of the γ band induced by the rotation of the octahedra.[40–42] Wang *et al.*[40] report a holelike γ band for $x = 0.5$, in agreement with the theory and magnetoresistance oscillations.[43] However, for even smaller Sr content, in the doping range where the tilt distortion is also present, $x = 0.2$, Neupane *et al.*[42] report the complete disappearance of the γ-Fermi surface sheet, whereas Shimoyamada *et al.*[41] find that all bands cross the Fermi level for this concentration. All three ARPES studies[40–42] clearly document that the d_{xy} states are strongly renormalized. The γ-band width around the wave vectors associated with the van Hove singularity, (0.5,0,0), is remarkably small; it amounts to only a few meV,[41] similar to the values reported for $Sr_3Ru_2O_7$.[30] The extreme reduction of the γ-band width results in a high electronic density of states at the Fermi level, which manifests itself in the heavy-mass states[6,7] as well as in the remarkably strong thermal expansion anomalies in $Ca_{2-x}Sr_xRuO_4$ for $0.2 < x < 0.6$.[44]

Besides the signals at $Q^{IC}_{\alpha\beta}$, all magnetic correlations observed in our INS experiments should be attributed to the γ band. The amplitude of the incommensurate signal at Q^{IC}_1 and Q^{IC}_2 in $Ca_{1.38}Sr_{0.62}RuO_4$ (Ref. 19) is three times larger than that of the incommensurate nesting signal in pure Sr_2RuO_4.[17] The rotational distortion of the structure should have a relatively small effect on the d_{xz} and d_{yz} bands, so it appears very unlikely that the magnetic signal associated with these bands changes so drastically between Sr_2RuO_4 and $Ca_{1.38}Sr_{0.62}RuO_4$. This conclusion is corroborated by the fact that the $Q^{IC}_{\alpha\beta}$ signal, which can unambiguously be attributed to these bands, remains constant between $x = 2$ and $x = 0.2$. As there is little change in the Q^{IC}_1 and Q^{IC}_2 signals for $x = 0.2$ and 0.62, it appears reasonable to assume that for $x = 0.2$ this incommensurate scattering does not arise from the $d_{xz}$and d_{yz} bands either. Although the ferromagnetic fluctuations originate from the γ band and the high density of states at the Fermi level, it is still possible that some sections of the γ surface are at the same time responsible for the signals at Q^{IC}_1 and Q^{IC}_2.[32] In a very simple approach, the holelike Fermi surface for $x = 0.5$ (Refs. 19, 37, and 40) may explain a peak in the Lindhard susceptibility associated with electron transfer from $(0.5, +\delta, 0)$ to $(0.5, -\delta, 0)$ and thereby an incommensurate signal on the tetragonal axes, but for any quantitative statement the knowledge about the electronic structure in $Ca_{1.5}Sr_{0.5}RuO_4$ is clearly insufficient.

B. Contribution of the spin fluctuations to the electronic specific heat

As do other excitations, the incommensurate magnetic fluctuations contribute to the specific heat. Their contribution to the coefficient of the electronic specific heat at low temperature can be approximated as[45]

$$\gamma_{sf} = \frac{\pi k_B^2}{\hbar} \sum_q \frac{1}{\Gamma(q)}, \tag{5}$$

where the sum is over the whole Brillouin zone. Performing a very simple estimation (taking Γ constant in an area defined by the widths of the peaks) with the fitted parameters for $Ca_{1.8}Sr_{0.2}RuO_4$ yields 160 mJ/mol K^2, which is reasonably near the directly measured value[7] of 175 mJ/mol K^2 and proves that the remarkably high electronic specific heat can be understood in terms of the magnetic fluctuations. For $Ca_{1.38}Sr_{0.62}RuO_4$, in which the coefficient of the electronic specific heat has the even higher value of 250 mJ/mol K^2, an analogous estimation has already been performed,[19] yielding perfect agreement, $\gamma_{sf} = 250$ mJ/mol K^2.

In view of the similarity of the incommensurate fluctuation spectrum of both Sr concentrations, it appears reasonable to assume that their contribution to γ_{sf} is approximately equal. The main difference between $Ca_{1.38}Sr_{0.62}RuO_4$ and $Ca_{1.8}Sr_{0.2}RuO_4$ is the presence of the ferromagnetic component; the different value of the specific heat coefficient therefore gives a rough estimate for the contribution of the ferromagnetic fluctuations to the specific heat.

C. Model for the incommensurate fluctuations in $Ca_{1.8}Sr_{0.2}RuO_4$

As the full band-structure-based analysis of the magnetic excitations seems impossible at the moment, we develop a model based on the general expressions derived in Sec. II. The antiferromagnetic correlations can be described more easily in the case of $Ca_{1.8}Sr_{0.2}RuO_4$, as there is no ferromagnetic part to be taken into account at low temperature.

Using Eqs. (2) and (4) for fluctuations close to a general incommensurate antiferromagnetic instability, one obtains, in a global fit to the available data, including the convolution

with the experimental resolution, a very good description of the incommensurate magnetic excitations at $Q_1^{\rm IC}$ and $Q_2^{\rm IC}$ in $Ca_{1.8}Sr_{0.2}RuO_4$. To account for the two inequivalent wave vectors, each of them is assumed to contribute according to these equations, and the contributions of these and the symmetrically equivalent positions in the Brillouin zone are simply summed up. As the widths are large, this implies a quite significant overlap of these signals, which prohibits the separation of the individual contributions. Γ_0 and ξ are thus set equal for both parts. It turns out that ξ can be taken as isotropic in the plane. Note that we may neglect the orthorhombic distortion as the tetragonal [100] and [010] directions remain equivalent in the orthorhombic lattice. Finally, we do not take into account any anisotropy of the fluctuations in spin space—in general, though, one would expect that in an anisotropic system only one component of the fluctuations diverges when approaching the magnetic instability. The geometric effect when measuring in different orientations indicates that these fluctuations are mainly polarized in the plane, i.e., χ''_{ab} is significantly larger than χ''_c in contrast to the finding for the nesting signal at $Q_{\alpha\beta}^{\rm IC}$ in pure Sr_2RuO_4.[22]

The parameters that we use to describe the spin fluctuations in $Ca_{1.8}Sr_{0.2}RuO_4$ at low temperature are $q_1 = 0.12 \pm 0.01$, $q_2 = 0.27 \pm 0.01$, $\Gamma_0 = 2.7 \pm 0.2$ meV, and $\xi = 5.9 \pm 0.3$ Å. The latter value corresponds to less than twice the lattice spacing and shows that these correlations still exhibit a very short length scale, even shorter than that of the fluctuations at $Q_{\alpha\beta}^{\rm IC}$ in Sr_2RuO_4.[18,21]

VI. FERROMAGNETIC CORRELATIONS

A. Low-frequency ferromagnetic fluctuation

In addition to the incommensurate scattering, there is clear evidence for truly ferromagnetic scattering in $Ca_{1.8}Sr_{0.2}RuO_4$ (Ref. 31) as well as in $Ca_{1.38}Sr_{0.62}RuO_4$. In Fig. 3 we summarize the results of constant energy scans at an energy transfer of 0.4 meV in $Ca_{1.38}Sr_{0.62}RuO_4$. The constant-Q scans were performed at $Q^{\rm FM} = (0,0,1.6)$, which is equivalent to a ferromagnetic zone center for 2D scattering. The results of single-relaxor fits are given in Fig. 4. By scanning the L component, i.e., along $(0,0,L)$ at 10 K and at a constant energy transfer of 0.4 meV, we have verified that there is no variation of the amplitude of the signal as function of L apart from that owing to the magnetic form factor, documenting the 2D nature of this signal.

It is evident at all temperatures that the scattering is maximum at $Q^{\rm FM}$, and there is no indication of any further scattering at the incommensurate wave vectors. This is consistent with the presence of the incommensurate fluctuations in $Ca_{1.38}Sr_{0.62}RuO_4$, as these are known to have a much higher characteristic energy of ~2.5 meV.[19] Note that in Fig. 3 the signal has already been corrected for the Bose factor, yielding a quantity that is (neglecting resolution effects) proportional to the imaginary part of the susceptibility. This reveals well the pronounced temperature dependence.

In Fig. 3(c) we show fits with a single-relaxor function (2). This function provides a good description of the signal and allows one to extract the characteristic energy of the signal and the real part of the susceptibility at zero frequency,

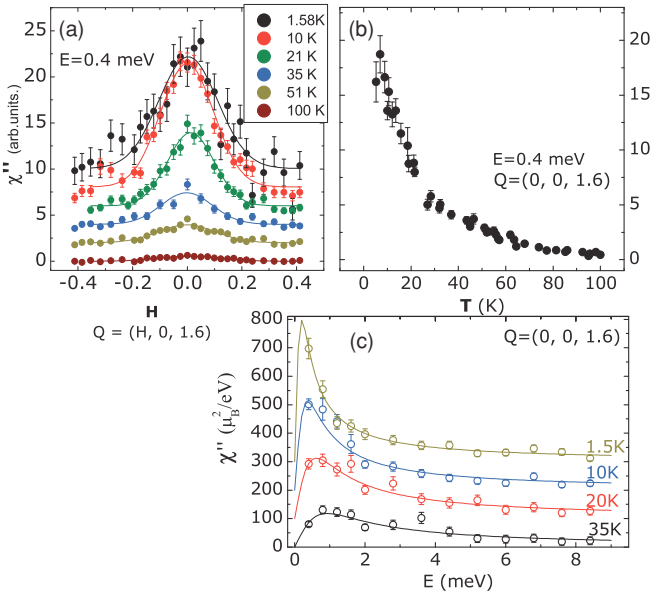

FIG. 3. (Color online) Magnetic scattering in $Ca_{1.38}Sr_{0.62}RuO_4$ taken around the FM wave vector (0,0,1.6) on the 4F spectrometer. (a) Constant energy scans at different temperatures. Shifted by two units each. (b) Signal at (0,0,1.6) as a function of temperature. (c) Signal as a function of energy at different temperatures (shifted by $100\mu_B^2$/eV each). Lines are fits to a single-relaxor function (see text).

which corresponds to the macroscopic susceptibility. Figure 4 contains the results for these parameters, which are both strongly temperature dependent: The characteristic energy reaches values as low as 0.2 meV at low temperatures, which is an order of magnitude lower than the values found for the incommensurate scattering, and which explains that this signal has not been observed in the previous studies[19] that focused on a higher-energy range. The susceptibility reaches very high values at low temperatures, but remains finite. In this context, let us mention that the unit μ_B^2/eV per ruthenium atom corresponds to 3.23×10^{-5} emu mol^{-1} in cgs units and (for the given volume of the unit cell) to 7.102×10^{-6} in SI. The obtained values agree with the bulk measurement in view of the uncertainties related to the calibration process. The value at low temperatures is less exact because the characteristic energy is so low that the maximum as function of energy transfer could

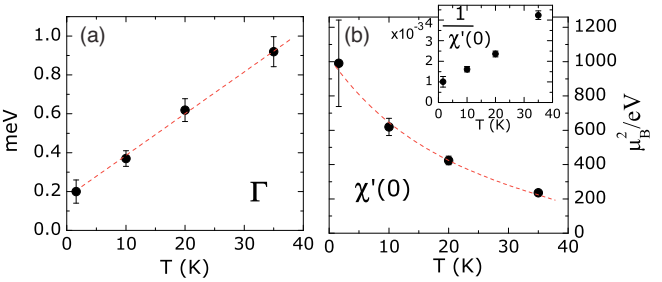

FIG. 4. (Color online) Analysis of FM scattering in $Ca_{1.38}Sr_{0.62}RuO_4$. (a) Characteristic energy, as obtained from the fits in Fig. 3. (b) Value of the real part of the macroscopic susceptibility, calibrated to absolute units, obtained from the same fits. (Inset: Inverse of the same values.)

not be well captured by the neutron measurement [Fig. 3(c)]. The good agreement with the macroscopic susceptibility shows that these fluctuations are indeed the relevant ones for the observed magnetic properties, in particular, for the metamagnetism.

When approaching a transition to an ordered state from above the critical temperature, it is expected that the characteristic energy of the fluctuations approaches zero and that the susceptibility diverges such that χ^{-1} vanishes. The evolution of Γ and χ qualitatively agrees with a transition to a ferromagnetic state. However, the transition is not reached at finite temperatures, as the extrapolation of Γ and χ^{-1} would reach zero at $\sim$10 K below zero temperature. At the temperature of 50 mK there is no indication of magnetic order in $Ca_{1.38}Sr_{0.62}RuO_4$ [nor in $Ca_{1.5}Sr_{0.5}RuO_4$ (Ref. 19)], and the amplitude of the fluctuations is consistent with the just discussed temperature evolution. This behavior can be compared to that of the incommensurate scattering in Sr_2RuO_4, which also indicates a magnetic transition that is not reached at finite temperature.[17] In both cases the blocking of the transition at low temperature may be connected with a reduction in the electrical resistivity. In $Ca_{1.38}Sr_{0.62}RuO_4$ the suppression of the phase transition at low temperature may be further related to the thermal expansion anomaly, which, although being much weaker compared to that in $Ca_{1.8}Sr_{0.2}RuO_4$, is still sizable in $Ca_{1.38}Sr_{0.62}RuO_4$.[44]

B. Model for incommensurate and ferromagnetic fluctuations in $Ca_{1.38}Sr_{0.62}RuO_4$

When using the corresponding equations (2) and (3), the fit of the ferromagnetic component is not satisfactory, contrary to the description of the incommensurate fluctuations. The reason is that it cannot account for the observed finite energy of the excitation in the zone center of approximately $\Gamma_0 = 0.2$ meV, as discussed above (see, for instance, Figs. 3 and 4), and the resulting maximum at $H = 0$ in the scans at low-energy transfers in Fig. 5. According to (2) and (3), $\chi''(\omega)$ is zero for $q = 0$, reflecting the conservation of total magnetization in the simple underlying model. In the presence of spin-orbit coupling, for instance, this is no longer required, although it is not evident how to modify Eq. (3). Another physical reason for the finite energy at $q = 0$ may be that, close to the magnetic instability, which is actually three dimensional (3D), the assumption of purely 2D fluctuations is no longer strictly correct, or in other words, the correlation length along c is no longer zero. This latter effect may be straightforwardly included in (3) and produces a better description of the data (lines in Fig. 5). The value $\xi^c_{\rm fm} \simeq 2$ Å is only a phenomenological parameter, and a more significant reason for the finite Γ at the zone center is likely to be the spin-orbit interaction. In this context we mention that a similar effect has been observed in the paramagnetic states of UGe_2,[46] a strongly anisotropic Ising ferromagnetic metal, in UPt_3,[47] and in MnP.[48]

With the modification of a finite Γ at the zone center, the overall description of the entire data set taken at $T = 1.5$ K is satisfactory for $Ca_{1.38}Sr_{0.62}RuO_4$. For the incommensurate parts, Γ_0 is 2.5 ± 0.2 meV and $\xi = 9.5 \pm 0.5$ Å. For the ferromagnetic component, the energy scale is much lower,

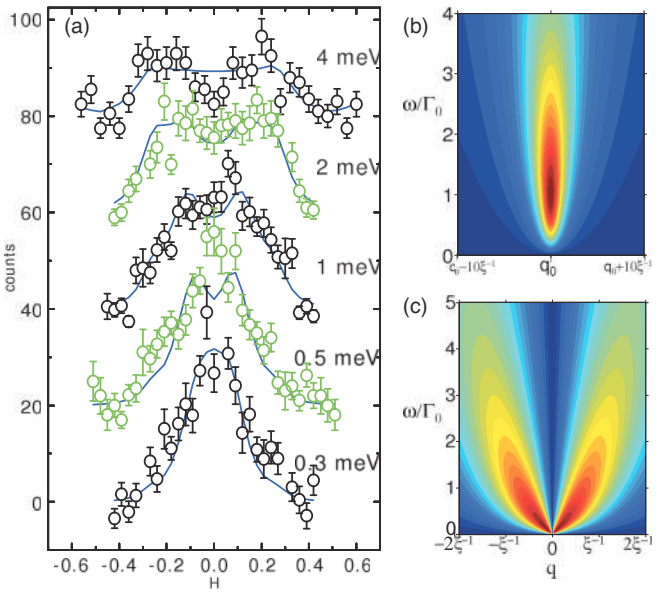

FIG. 5. (Color online) Magnetic scattering in $Ca_{1.38}Sr_{0.62}RuO_4$ ($T = 0.05$ K, shifted by 20 counts each). The model used to fit the data in (a) consists of a ferromagnetic contribution and two incommensurate antiferromagneticlike excitations at $Q_1^{\rm IC}$ and $Q_2^{\rm IC}$. These components are given by Eqs. (2)–(4) and are displayed separately in (b) and (c). The ferromagnetic one has to be modified to account for the measured finite energy at the zone center. Data taken on the IN14 spectrometer.

as already discussed, $\Gamma_0 = 0.34 \pm 0.05$ meV, but the in-plane correlation length is very short, $\xi^{ab}_{\rm FM} = 4.2 \pm 0.3$ Å.

The data in Fig. 4 can be described by a simple temperature variation of χ and Γ_0, including an offset temperature,

$$\chi(T) = \frac{C}{T + \Theta} \quad \text{and} \quad \Gamma_0(T) = G(T + \Theta), \tag{6}$$

with constants C and G. When combining these expressions with the energy spectrum (2), one obtains $\chi''(\omega, T) = C\frac{\omega G}{\omega^2 + G^2(T+\Theta)^2}$, so it follows

$$\omega\chi''(\omega, T) = f\left(\frac{\omega}{T + \Theta}\right), \tag{7}$$

with the function $f(x) = C\frac{x^2}{x^2+G^2}$. When plotting $\omega\chi''$ against $\omega/(T + \Theta)$, the data should thus fall on a single curve. In Fig. 6 this is performed for the ferromagnetic fluctuations in $Ca_{1.38}Sr_{0.62}RuO_4$ [data from Figs. 3(b) and 3(c)], which thereby are described as functions of temperature and energy. Note, however, that although resembling the Curie-Weiss susceptibility of an antiferromagnet, the meaning of the temperature offset Θ is quite different in Eq. (6), where the susceptibility at the magnetic instability is treated, whereas the antiferromagnetic Curie-Weiss law describes the macroscopic (ferromagnetic) susceptibility for an antiferromagnetic instability.

The analysis in Fig. 4 allows one to obtain the values for the constants C, G, and Θ. We use $G_{\rm FM} = 0.021$ meV$/K$ and $\Theta_{\rm FM} = 10$ K. In the Curie-Weiss law, the constant C is related to the magnetic moment, $C = \frac{n\mu_0\mu^2_{\rm eff}}{3k_B}$ (n being the number of magnetic moments per volume). Assuming a free local spin

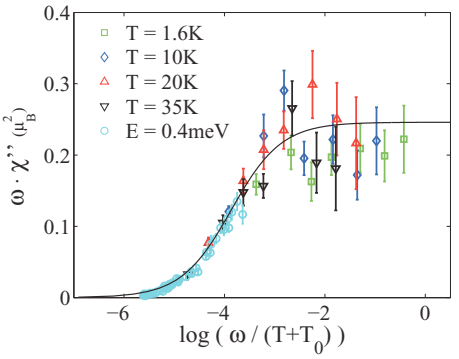

FIG. 6. (Color online) Ferromagnetic fluctuations in $Ca_{1.38}Sr_{0.62}RuO_4$: Different data sets taken at constant temperature or energy transfer (same as in Fig. 3). The quantity $\omega\chi''$ only depends on $\omega/(T+\Theta)$. The line is the function f for the parameter values discussed in the text.

$\frac{1}{2}$ per ruthenium atom, one calculates $C = 11\,729\mu_B^2/\text{eV K}$ comparable to the value of $\sim$11 400 $\mu_B^2/\text{eV K}$ found in Fig. 4. This analysis further illustrates the strength of the magnetic scattering in $Ca_{1.38}Sr_{0.62}RuO_4$.

For the incommensurate fluctuations, the analysis[19] provides $G_{IC} = 0.1$ meV/K and $\Theta_{IC} = 25$ K. C_{IC} is, to an estimated accuracy of $\sim$10%, 12 000 $\mu_B^2/\text{eV K}$, practically the same as C_{FM}, again documenting the strength of the magnetic correlations.

Furthermore, with this parameter set it is possible to describe the interplay of ferromagnetic and incommensurate fluctuations as a function of temperature. Θ indicates how far the system at $T = 0$ is still away from the hypothetical magnetic instability and the divergence of the fluctuations. As Θ is larger for the incommensurate correlations, they are less temperature dependent in the low-temperature range. Experimentally, the spin fluctuations (though broadened and with higher background) can be observed up to room temperature, because the Bose thermal factor [Eq. (1)] roughly compensates the decreasing magnitude of χ (see Fig. 7). The basic qualitative consequence of the temperature variation (6) is that the balance between the incommensurate and ferromagnetic parts changes considerably depending on the temperature and on the energy transfer of the scan. For the given parameters and the relaxor spectrum (2) it follows, for instance, that $\chi''_{FM}(\omega,T) > \chi''_{IC}(\omega,T)$ under the condition $T > 25\frac{K}{meV}\hbar\omega - 30$ K, i.e., at high temperatures and/or low-energy transfer one predominantly measures the ferromagnetic fluctuations. This effect is well confirmed for $x = 0.62$ by a series of scans at various temperatures up to 240 K and energy transfers up to 8 meV (see Fig. 7). Qualitatively, the same effect is also observed for $x = 0.2$ at higher temperatures (see Fig. 8 and below).

C. Suppression of ferromagnetic fluctuations at $x = 0.2$

Also, $Ca_{1.8}Sr_{0.2}RuO_4$ exhibits ferromagnetic excitations, but in contrast to $Ca_{1.38}Sr_{0.62}RuO_4$, they are almost entirely suppressed at low temperatures. Figure 8 summarizes the corresponding scans at 1.5 and 10 K. One might argue whether the central intensity can arise from the overlap of

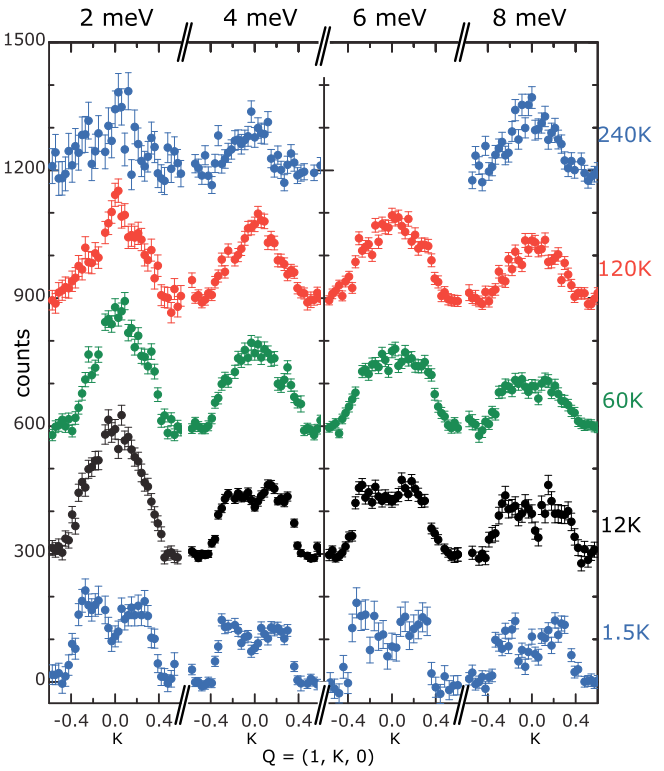

FIG. 7. (Color online) Magnetic scattering in $Ca_{1.38}Sr_{0.62}RuO_4$ as a function of temperature and energy (background subtracted, shifted by 300 counts each). All constant energy scans along $Q = (1,K,0)$ were performed on the thermal triple-axis spectrometer 1T. The signal changes its shape qualitatively owing to the interplay of ferromagnetic and incommensurate contributions. At high energy and low temperature the incommensurate signals dominate, whereas at low energy and high temperature the centered peak in these scans arises from the ferromagnetic component.

the incommensurate contributions just at the ferromagnetic wave vector. The data taken at higher temperatures and higher-energy transfers unambiguously exclude this picture. Figure 8(e) shows data taken at $T = 65$ K for $x = 0.2$. For comparison with low temperature, the blue line shows the shape of the signal at $T = 2$ K. It is impossible to ascribe the shape of the high-temperature data only to a broadening; even for less sharp central maxima, a broadening would need to be extreme to account for a maximum at $K = 0$ (green line). Instead, it can be very easily reproduced by simply adding an additional signal at $K = 0$, such as the one in Fig. 3(a), to the low-temperature data. The incommensurate part of the scan is thus essentially unchanged, and the difference between high and low temperature has to be ascribed entirely to the appearance of an additional ferromagnetic component. Therefore, also the susceptibility analysis and its temperature dependence has to be interpreted as owing to changes in the intrinsically ferromagnetic correlations and not to changes in the antiferromagnetic ones.

The temperature dependence of the amplitude of the ferromagnetic signal is in good quantitative agreement with the macroscopic susceptibility, as has already been discussed in Ref. 31. The characteristic energies Γ are, at the higher temperatures, of the same order as in $Ca_{1.38}Sr_{0.62}RuO_4$. For

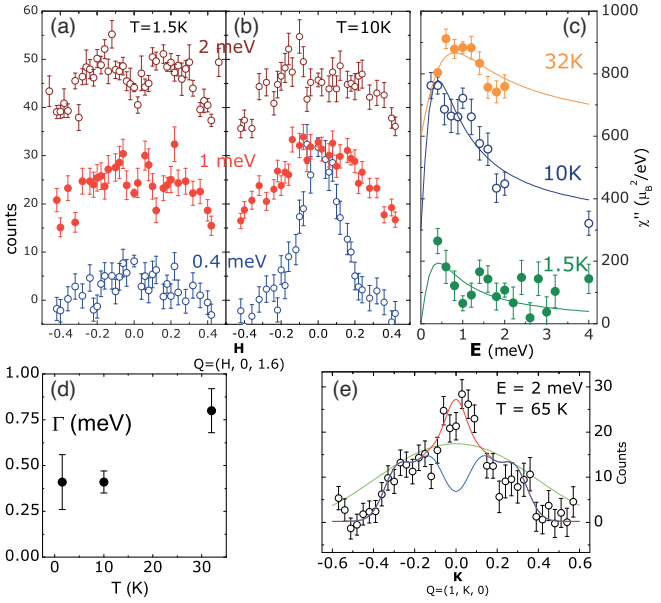

FIG. 8. (Color online) Ferromagnetic scattering in $Ca_{1.8}Sr_{0.2}RuO_4$. (a) and (b) Scans across Q^{FM} at different energy transfers and temperatures. (c) Energy dependence at Q^{FM} and fits with a relaxor function (shifted by 20 counts and $300\mu_B^2$/eV, respectively). (d) Characteristic energy Γ of the signal at Q^{FM}. (e) Additional ferromagnetic contribution at $T = 65$ K: The blue line is the fit to the corresponding scan at $T = 2$ K. For demonstration purposes, the green curve shows a Gaussian broadening of the blue curve, which can produce a maximum at $K = 0$, but only for parameters that fail to describe the full scan. The red line is the sum of the blue $T = 2$ K curve and a Gaussian peak at $K = 0$.

$x = 0.2$, however, it is obvious that the relatively simple picture of approaching a magnetic instability cannot be maintained until low temperature. This is in accordance with other anomalous effects that take place in this temperature region, in particular, the remarkable anomalous structural evolution.[44] A deformation of the lattice and the environment of the ruthenium ions occurs, which likely couples to its electronic configuration, thereby suppressing the ferromagnetic instability. It is worthwhile to note that these effects are also present in $Ca_{1.38}Sr_{0.62}RuO_4$, although to a much weaker extent.[44] The close inspection of $\frac{1}{\chi'(0)}$ shown in the inset of Fig. 4(b) suggests that also in $Ca_{1.38}Sr_{0.62}RuO_4$ the emergence of the ferromagnetic instability is damped by the same mechanism, but to a smaller extent.

VII. MAGNETIC-FIELD EFFECT

At Sr concentrations lower than $x = 0.5$, $Ca_{2-x}Sr_xRuO_4$ shows a metamagnetic transition[8] that manifests itself as a steep nonlinear increase of magnetization as a function of the external magnetic field. The metamagnetic transition in $Ca_{1.8}Sr_{0.2}RuO_4$ has been well characterized by a number of different techniques (see, for instance, Refs. 7, 43, 44, and 50). In particular, the inelastic neutron scattering study[31] has revealed the appearance of an excitation mode that resembles a magnon in a conventional ferromagnet. This proves that—whatever are its microscopic mechanism and the thermodynamic details—a substantial ferromagnetic interaction is induced at the metamagnetic transition. $Ca_{1.38}Sr_{0.62}RuO_4$ does not show a clear metamagnetic transition, but its high susceptibility still resembles the peak at the transition of the samples that are metamagnetic, so that one might argue that it behaves similar to the high-field state of $Ca_{1.8}Sr_{0.2}RuO_4$. To further study the (ferro-)magnetic interactions in both systems, and in particular compare the ones induces by a field to those present in zero field in $Ca_{1.38}Sr_{0.62}RuO_4$, we have applied a magnetic field. A field of 10 T is sufficient to be safely above the metamagnetic transition in $Ca_{1.8}Sr_{0.2}RuO_4$ and suppress the remainders of the low-field incommensurate signals. Choosing the same field value for $Ca_{1.38}Sr_{0.62}RuO_4$ permits to compare both systems under the same conditions.

The effect of the magnetic field on the zone-center fluctuation is compared for $Ca_{1.8}Sr_{0.2}RuO_4$ and $Ca_{1.38}Sr_{0.62}RuO_4$ in Fig. 9. In both cases the zero-field response (which is very weak for $Ca_{1.8}Sr_{0.2}RuO_4$) is shifted to higher energies. The spectrum is then qualitatively different and a description using the relaxor function (2) is no longer possible.

The energy $g\mu_B B$, which is the Zeeman energy of an electron in the magnetic field, amounts to $\sim$1.15 meV for $B = 10$ T. The spectral form at 10 T can indeed be well described by a Lorentzian function $\Gamma/[(\omega-\omega_0)^2+\Gamma^2] - \Gamma/[(\omega+\omega_0)^2+\Gamma^2]$ with $\omega_0 = 1.15$ meV, the broadening, though, being extreme (heavily overdamped) in the case of $Ca_{1.38}Sr_{0.62}RuO_4$. A quantitative comparison of the widths is not straightforward because the different crystal orientation in both cases means that the experimental resolution and the averaging of the susceptibility components is not the same. The shift of spectral weight to higher energy is qualitatively the same for both concentrations. Not knowing if the excitation in $Ca_{1.38}Sr_{0.62}RuO_4$ disperses in the same way as in $Ca_{1.8}Sr_{0.2}RuO_4$, it is likely that the spin correlations are weaker, as is consistent with the larger width, and

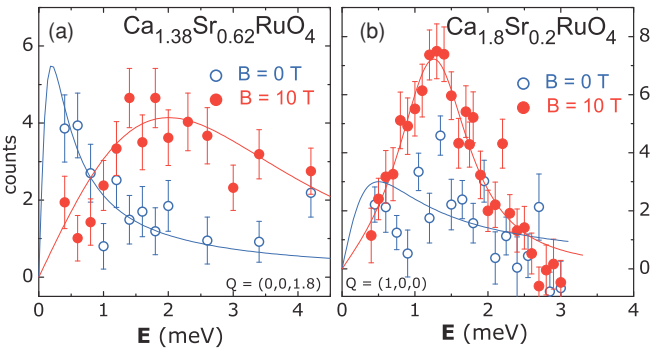

FIG. 9. (Color online) Effect of a magnetic field on the ferromagnetic fluctuations in (a) $Ca_{1.38}Sr_{0.62}RuO_4$ and (b) $Ca_{1.8}Sr_{0.2}RuO_4$. The temperature is 1.5 K and the background has been subtracted in both cases (but the scales are not normalized to each other). Lines correspond to a single relaxor ($B = 0$, with the characteristic energies discussed in the text) and to Lorentzian functions ($B = 10$ T), respectively. The 0 T data in (b) have been measured with low statistics only, in order to fix the intensity scale relative to the high-field data under the same experimental conditions. To determine their spectral shape and energy scale, we use the information from the previously discussed zero-field data. The data were taken on the (a) IN12 and (b) Panda spectrometers.

in accordance with the lower magnetic moment at 10 T compared to $Ca_{1.8}Sr_{0.2}RuO_4$ ($0.4\mu_B$ vs $0.6\mu_B$). The ratio of the susceptibilities obtained by a Kramers-Kronig analysis $\chi' = \int \chi''(\omega)/\omega\, d\omega$ from the data in Fig. 9(a) ($\chi_{0\,\mathrm{T}}/\chi_{10\,\mathrm{T}} \simeq 1.8$) is consistent with the ratio of the susceptibilities from the macroscopic measurement. In $Ca_{1.8}Sr_{0.2}RuO_4$, in addition, taking into account the data at intermediate fields,[31] the corresponding analysis perfectly describes the susceptibility maximum at the metamagnetic transition near 3 T.

With the high-field data obtained for $x = 0.2$ it is also possible to provide a more detailed characterization of the magnon mode at $B = 10$ T. Because it rapidly broadens and weakens with increasing energy, it can best be studied between 1 and 3 meV; Fig. 10(a) displays data taken in this energy range. The positions of the maxima fall on a quadratic dispersion curve, with a gap of 1.15 meV as displayed in Fig. 10(b), i.e.,

$$\hbar\omega_q = \Delta + Dq^2, \tag{8}$$

with $D = 47 \pm 5$ meV Å^2.

It is, however, evident from the scans and from the color plot of the intensity in Fig. 10(c) that there is significant broadening of the magnon mode in q and ω. This broadening cannot be explained by the resolution of the spectrometer, but it is intrinsic. We have found that it is possible to describe the data with the usual Lorentzian energy spectrum,

$$\chi''(q,\omega) \propto \frac{\Gamma_q}{(\omega-\omega_q)^2+\Gamma_q} - \frac{\Gamma_q}{(\omega+\omega_q)^2+\Gamma_q^2}, \tag{9}$$

where ω_q follows Eq. (8). It is necessary, though, to include an additional parameter that accounts for the broadening and the decrease of intensity toward higher energy—this decrease might be owing to an approach to the Stoner

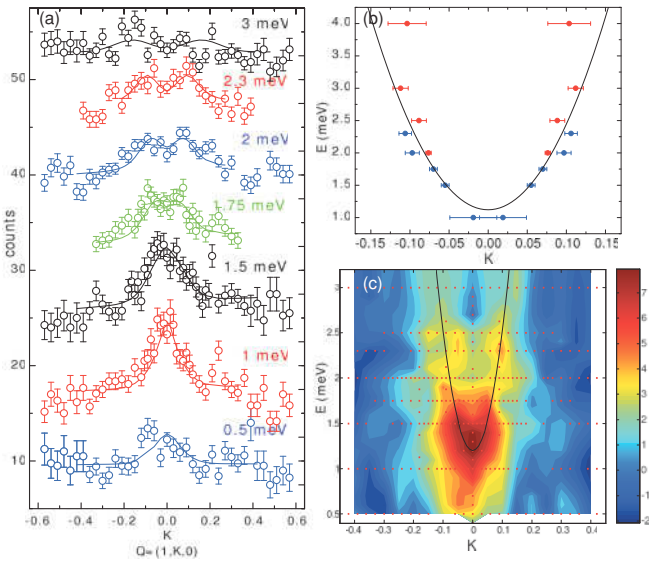

FIG. 10. (Color online) Magnetic excitations in $Ca_{1.8}Sr_{0.2}RuO_4$ at $B = 10$ T ($B \parallel c$ and $T = 1.5$ K). (a) Transverse scans through (1,0,0) at different energy transfers (shifted by 7.5 counts each). The lines are fits to the model described in the text. (b) Dispersion of the magnon, extracted from fits to the scans in (a) with symmetric Gaussian peaks. Red data points are taken from Ref. 31. (c) Colour plot of the data in (a) (background subtracted).

continuum, where the intensity of the magnon is expected to disappear.[11,12] Allowing Γ_q to vary as $\Gamma_q = \Gamma_0 + cq$, one introduces an additional parameter c that contains a length scale and that can be considered as modeling an effective finite spatial correlation. With this model, it is possible to perform a global fit to all the data that have been taken, including the resolution function of the spectrometer. The results are $\Delta = 1.16 \pm 0.03$ meV, $\Gamma_0 = 0.55 \pm 0.04$ meV, $c = 5.6 \pm 0.5$ meV Å, and $D = 34 \pm 2$ meV Å^2. Note that Δ, although unconstrained, corresponds well to $g\mu_B B = 1.15$ meV, which means that anisotropy terms are either unimportant or they effectively average out, and that D is different from the value given above because the new parameter c shifts the maxima in the constant energy scans with respect to the curve defined by (8).

VIII. CONCLUSIONS

The comprehensive INS studies provide a detailed description of the magnetic correlations in $Ca_{2-x}Sr_xRuO_4$. Different types of magnetic fluctuations are identified: We can separate a ferromagnetic signal and different features at incommensurate Q vectors—one on the diagonal of the Brillouin zone at $Q^{\mathrm{IC}}_{\alpha\beta} = (0.3,0.3,0)$ and a broader and stronger contribution on the $a^\star/b^\star$ axis. This latter one has an internal structure that can be well described by assuming two overlapping contributions from $Q^{\mathrm{IC}}_1 = (0.11,0,0)$ and $Q^{\mathrm{IC}}_2 = (0.26,0,0)$ and equivalent positions. Within the accuracy of the measurement—limited primarily by the large overlap of the signals—there is no significant difference in the Q positions of these contributions for the different values of the Sr concentration $x = 0.2$ and $x = 0.62$. The signal at $Q^{\mathrm{IC}}_{\alpha\beta}$ can be associated with the incommensurate signal in Sr_2RuO_4.[18] As its origin is well understood arising from nesting of the α and β Fermi surface, the presence of this signal at the same position indicates that these sheets of the Fermi surface, and thus also the occupation of the ruthenium d_{xz} and d_{yz} orbitals, are only slightly changed in $Ca_{2-x}Sr_xRuO_4$ ($x = 0.2/0.62$) with respect to Sr_2RuO_4.[41] The origin, i.e., the relevant sections of the Fermi surface, of the signals at $Q^{\mathrm{IC}}_1/Q^{\mathrm{IC}}_2$ is not yet precisely identified, but for several reasons they are most likely related to the γ sheet of the Fermi surface. ARPES measurements and band-structure calculations clearly identify the γ band as the highly renormalized one associated with a heavy-mass electronic behavior and with a high susceptibility, but a detailed structure of the γ sheet awaits further studies.

There seems to be no significant change of the different incommensurate components for $x = 0.2$ and $x = 0.62$, which is thus presumably the case for the whole range $0.18 \leqslant x \leqslant 1.5$. Although the temperature dependence of χ and Γ of these fluctuations[19] indicates that the system approaches a magnetic instability at incommensurate ordering vectors, the system obviously can be considered as still sufficiently far away and not directly in the critical region. The structural and other variations in this range of x do not very sensitively couple to this part of the magnetic correlations. The rotational structural distortion, however, is apparently very important and causes a significant difference in Sr_2RuO_4, where no excitations are observed at Q^{IC}_1 or Q^{IC}_2. It is remarkable that in the bilayer

material $Sr_3Ru_2O_7$ very similar excitations as at Q_1^{IC} and Q_2^{IC} have been observed.[24,26] In view of the similar $Sr_3Ru_2O_7$ crystal structure, which also exhibits the rotational distortion,[49] this appears consistent. These two layered ruthenates and their metamagnetic transitions appear to be very similar to each other.

The incommensurate fluctuations at Q_1^{IC}/Q_2^{IC} have a characteristic energy of ~2.7 meV, while the characteristic energy of the excitations at the zone center is only 0.4 meV at $T =$ 10 K in $Ca_{1.8}Sr_{0.2}RuO_4$. In $Ca_{1.38}Sr_{0.62}RuO_4$ this latter value further decreases to 0.2 meV at $T = 1.5$ K and the amplitude increases, consistent with the picture of $Ca_{1.38}Sr_{0.62}RuO_4$ approaching a ferromagnetic instability, although not reaching it at finite temperatures. In $Ca_{1.8}Sr_{0.2}RuO_4$, the ferromagnetic part of the response is strongly suppressed at low temperature. The values of the susceptibility related to the ferromagnetic signal are, concerning their absolute values as well as their variations with temperature and magnetic field, in perfect agreement with the macroscopically determined susceptibilities, proving that this INS signal reflects the magnetic correlations that determine the macroscopic physical properties.

The application of an external magnetic field at low temperature suppresses the incommensurate part of the response. In $Ca_{1.8}Sr_{0.2}RuO_4$, a substantial ferromagnetic component reappears, reflecting the metamagnetic transition. At high field, the spectral weight of the ferromagnetic response is shifted toward higher energy for $x = 0.2$ and 0.62, opening a gap that roughly corresponds to the Zeeman energy of an electron in the magnetic field. In $Ca_{1.8}Sr_{0.2}RuO_4$ a dispersive excitation mode, corresponding to a magnon in a ferromagnet, is observed, which is well defined near the zone center and low energies, and which significantly broadens at energies above 3 meV.

Although only two concentrations have been studied here, $x = 0.2$ and 0.62, the results are most likely of relevance for the whole range $0.2 \leqslant x \leqslant 1.5$ of the series $Ca_{2-x}Sr_xRuO_4$. In this region of the phase diagram, the materials are paramagnetic and metallic at all temperatures. Nevertheless, as there is a second-order structural phase transition (associated with RuO_6 octahedra tilting), the samples with $x = 0.2$ and 0.62 have to be regarded as quite different in their physical properties; $Ca_{2-x}Sr_xRuO_4$ seems to approach the ferromagnetic instability for x decreasing toward 0.5, while a strongly reduced susceptibility and a metamagnetic transition are observed at $x < 0.5$. It is thus important to realize that the measured magnetic correlations can be well described in a common model in which a change in only a few parameters leads to the large differences between the nearly ferromagnetic and nearly antiferromagnetic compounds.

The ferromagnetic correlations in $Ca_{2-x}Sr_xRuO_4$ depend sensitively on the Sr concentration x and seem to tune the different magnetic properties with the doping. The ferromagnetic instability in general arises from the high density of states close to the Fermi surface of the γ sheet, which has been revealed in several ARPES studies.[40–42] Owing to this high density of states, the system becomes very sensitive upon structural changes, as it is best documented in the thermal expansion anomalies.[44,50]

In conclusion, the comprehensive INS experiments clearly reveal the image of competing magnetic instabilities in $Ca_{2-x}Sr_xRuO_4$. The whole spectrum of magnetic correlations is well described in the presented phenomenological model with ferromagnetic and incommensurate antiferromagnetic contributions. In this competition, it is mainly the variation of the ferromagnetic component as function of Sr concentration x, temperature, and magnetic field, that governs the physical properties.

ACKNOWLEDGMENT

This work was supported by the Deutsche Forschungsgemeinschaft through SFB 608.

*steffens@ill.eu
†Spektrometer PANDA, Institut für Festkörperphysik, TU Dresden, Germany.
‡braden@ph2.uni-koeln.de

[1] Y. Maeno, H. Hashimoto, K. Yoshida, S. Nishizaki, T. Fujita, J. G. Bednorz, and F. Lichtenberg, Nature (London) **372**, 532 (1994).
[2] A. P. Mackenzie and Y. Maeno, Rev. Mod. Phys. **75**, 657 (2003).
[3] S. Nakatsuji and Y. Maeno, Phys. Rev. Lett. **84**, 2666 (2000).
[4] S. Nakatsuji and Y. Maeno, Phys. Rev. B **62**, 6458 (2000).
[5] G. Cao, S. McCall, M. Shepard, J. E. Crow, and R. P. Guertin, Phys. Rev. B **56**, R2916 (1997).
[6] S. Nakatsuji, S. Ikeda, and Y. Maeno, J. Phys. Soc. Jpn. **66**, 1868 (1997).
[7] S. Nakatsuji, D. Hall, L. Balicas, Z. Fisk, K. Sugahara, M. Yoshioka, and Y. Maeno, Phys. Rev. Lett. **90**, 137202 (2003).
[8] S. Nakatsuji and Y. Maeno, J. Low Temp. Phys. **117**, 1593 (1999).
[9] R. S. Perry, L. M. Galvin, S. A. Grigera, L. Capogna, A. J. Schofield, A. P. Mackenzie, M. Chiao, S. R. Julian, S. Ikeda, S. Nakatsuji, Y. Maeno, and C. Pfleiderer, Phys. Rev. Lett. **86**, 2661 (2001).
[10] V. I. Anisimov, I. A. Nekrasov, D. E. Kondakov, T. M. Rice, and M. Sigrist, Eur. Phys. J. B **25**, 191 (2002).
[11] S. W. Lovesey, *Theory of Neutron Scattering from Condensed Matter*, Vol. 2 (Clarendon, Oxford, 1984).
[12] T. Moriya, *Spin Fluctuations in Itinerant Electron Magnetism* (Springer, Berlin, 1985).
[13] G. G. Lonzarich and L. Taillefer, J. Phys. C **18**, 4339 (1985).
[14] M. Kempa, B. Janousova, J. Saroun, P. Flores, M. Boehm, F. Demmel, and J. Kulda, Physica B **385-386**, 1080 (2006).
[15] O. Friedt, M. Braden, G. André, P. Adelmann, S. Nakatsuji, and Y. Maeno, Phys. Rev. B **63**, 174432 (2001).
[16] M. Braden, W. Reichardt, Y. Sidis, Z. Mao, and Y. Maeno, Phys. Rev. B **76**, 014505 (2007).
[17] M. Braden, Y. Sidis, P. Bourges, P. Pfeuty, J. Kulda, Z. Mao, and Y. Maeno, Phys. Rev. B **66**, 064522 (2002).
[18] Y. Sidis, M. Braden, P. Bourges, B. Hennion, S. Nishizaki, Y. Maeno, and Y. Mori, Phys. Rev. Lett. **83**, 3320 (1999).
[19] O. Friedt, P. Steffens, M. Braden, Y. Sidis, S. Nakatsuji, and Y. Maeno, Phys. Rev. Lett. **93**, 147404 (2004).

[20]F. Servant, S. Raymond, B. Fåk, P. Lejay, and J. Flouquet, Solid State Comm. **116**, 489 (2000).
[21]F. Servant, B. Fåk , S. Raymond, J. P. Brison, P. Lejay, and J. Flouquet, Phys. Rev. B **65**, 184511 (2002).
[22]M. Braden, P. Steffens, Y. Sidis, J. Kulda, P. Bourges, S. Hayden, N. Kikugawa, and Y. Maeno, Phys. Rev. Lett. **92**, 097402 (2004).
[23]T. Nagata, M. Urata, H. Kawano-Furukawa, H. Yoshizawa, H. Kadowaki, and P. Dai, Phys. Rev. B **69**, 174501 (2004).
[24]L. Capogna, E. M. Forgan, S. M. Hayden, A. Wildes, J. A. Duffy, A. P. Mackenzie, R. S. Perry, S. Ikeda, Y. Maeno, and S. P. Brown, Phys. Rev. B **67**, 012504 (2003).
[25]M. B. Stone, M. D. Lumsden, R. Jin, B. C. Sales, D. Mandrus, S. E. Nagler, and Y. Qiu, Phys. Rev. B **73**, 174426 (2006).
[26]S. Ramos, E. M. Forgan, C. Bowell, S. M. Hayden, A. J. Schofield, A. Wildes, E. A. Yelland, S. P. Brown, M. Laver, R. S. Perry, and Y. Maeno, Physica B **403**, 1270 (2008).
[27]I. I. Mazin and D. Singh, Phys. Rev. Lett. **79**, 733 (1997).
[28]C. Bergemann, A. Mackenzie, S. Julian, D. Forsythe, and E. Ohmichi, Adv. Phys. **52**, 639 (2003).
[29]D. J. Singh and I. I. Mazin, Phys. Rev. B **63**, 165101 (2001).
[30]A. Tamai, M. P. Allan, J. F. Mercure, W. Meevasana, R. Dunkel, D. H. Lu, R. S. Perry, A. P. Mackenzie, D. J. Singh, Z.-X. Shen, and F. Baumberger, Phys. Rev. Lett. **101**, 026407 (2008).
[31]P. Steffens, Y. Sidis, P. Link, K. Schmalzl, S. Nakatsuji, Y. Maeno, and M. Braden, Phys. Rev. Lett. **99**, 217402 (2007).
[32]E. Ko, B. J. Kim, C. Kim, and H. J. Choi, Phys. Rev. Lett. **98**, 226401 (2007).
[33]Z. Fang, N. Nagaosa, and K. Terakura, Phys. Rev. B **69**, 045116 (2004).
[34]Z. Fang and K. Terakura, Phys. Rev. B **64**, 020509(R) (2001).
[35]M. Braden, G. André, S. Nakatsuji, and Y. Maeno, Phys. Rev. B **58**, 847 (1998).
[36]E. Gorelov, M. Karolak, T. O. Wehling, F. Lechermann, A. I. Lichtenstein, and E. Pavarini, Phys. Rev. Lett. **104**, 226401 (2010).
[37]A. Liebsch and H. Ishida, Phys. Rev. Lett. **98**, 216403 (2007).
[38]A. Gukasov, M. Braden, R. J. Papoular, S. Nakatsuji, and Y. Maeno, Phys. Rev. Lett. **89**, 087202 (2002).
[39]J. S. Lee, S. J. Moon, T. W. Noh, S. Nakatsuji, and Y. Maeno, Phys. Rev. Lett. **96**, 057401 (2006).
[40]S.-C. Wang, H.-B. Yang, A. K. P. Sekharan, S. Souma, H. Matsui, T. Sato, T. Takahashi, C. Lu, J. Zhang, R. Jin, D. Mandrus, E. W. Plummer, Z. Wang, and H. Ding, Phys. Rev. Lett. **93**, 177007 (2004).
[41]A. Shimoyamada, K. Ishizaka, S. Tsuda, S. Nakatsuji, Y. Maeno, and S. Shin, Phys. Rev. Lett. **102**, 086401 (2009).
[42]M. Neupane, P. Richard, Z.-H. Pan, Y.-M. Xu, R. Jin, D. Mandrus, X. Dai, Z. Fang, Z. Wang, and H. Ding, Phys. Rev. Lett. **103**, 097001 (2009).
[43]L. Balicas, S. Nakatsuji, D. Hall, T. Ohnishi, Z. Fisk, Y. Maeno, and D. J. Singh, Phys. Rev. Lett. **95**, 196407 (2005).
[44]M. Kriener, P. Steffens, J. Baier, O. Schumann, T. Zabel, T. Lorenz, O. Friedt, R. Müller, A. Gukasov, P. G. Radaelli, P. Reutler, A. Revcolevschi, S. Nakatsuji, Y. Maeno, and M. Braden, Phys. Rev. Lett. **95**, 267403 (2005).
[45]T. Moriya and T. Takimoto, J. Phys. Soc. Jpn. **64**, 960 (1995); M. Hatatani and T. Moriya, J. Phys. Soc. Jpn. **64**, 3434 (1995).
[46]A. D. Huxley, S. Raymond, and E. Ressouche, Phys. Rev. Lett. **91**, 207201 (2003).
[47]N. Bernhoeft and G. Lonzarich, J. Phys. Condens. Matter **7**, 7325 (1995).
[48]K. Yamada, Y. Todata, Y. Endoh, Y. Ishikawa, P. Böni, and G. Shirane, J. Appl. Phys. **61**, 3400 (1987).
[49]H. Shaked, J. D. Jorgensen, O. Chmaissem, S. Ikeda, and Y. Maeno, J. Solid State Chem. **154**, 361 (2000).
[50]J. Baier, P. Steffens, O. Schumann, M. Kriener, S. Stark, H. Hartmann, O. Friedt, A. Revcolevschi, P. G. Radaelli, S. Nakatsuji, Y. Maeno, J. A. Mydosh, T. Lorenz, and M. Braden, J. Low Temp. Phys. **147**, 405 (2007).